

Feature-aligned Motion Transformation for Efficient Dynamic Point Cloud Compression

Xuan Deng^{1,2}, Xiandong Meng², Longguang Wang⁴, Tiange Zhang^{2,3},
Xiaopeng Fan^{1,2}, Debin Zhao^{1,2}

¹School of Computer Science and Technology, Harbin Institute of Technology

²Peng Cheng Laboratory, Shenzhen

³Peking University Shenzhen Graduate School, Shenzhen

⁴Sun Yat-sen University, Guangzhou

dengx01@pcl.ac.cn, Mengxd@pcl.ac.cn, wanglg9@mail.sysu.edu.cn, tgzhang@stu.pku.edu.cn,

fxp@hit.edu.cn, dbzhao@hit.edu.cn

Abstract

Dynamic point clouds are widely used in applications such as immersive reality, robotics, and autonomous driving. Efficient compression largely depends on accurate motion estimation and compensation, yet the irregular structure and significant local variations of point clouds make this task highly challenging. Current methods often rely on explicit motion estimation, whose encoded vectors struggle to capture intricate dynamics and fail to fully exploit temporal correlations. To overcome these limitations, we introduce a Feature-aligned Motion Transformation (FMT) framework for dynamic point cloud compression. FMT replaces explicit motion vectors with a spatiotemporal alignment strategy that implicitly models continuous temporal variations, using aligned features as temporal context within a latent-space conditional encoding framework. Furthermore, we design a random access (RA) reference strategy that enables bidirectional motion referencing and layered encoding, thereby supporting frame-level parallel compression. Extensive experiments demonstrate that our method surpasses D-DPCC and AdaDPCC in both encoding and decoding efficiency, while also achieving BD-Rate reductions of 20% and 9.4%, respectively. These results highlight the effectiveness of FMT in jointly improving compression efficiency and processing performance.

Introduction

A dynamic point cloud (DPC) is a sequence of point cloud frames, each consisting of unordered points sparsely distributed in 3D space (Xu et al. 2018). As a promising 3D data format, DPC finds broad applications in immersive media, volumetric capture, and AR/VR (Li et al. 2019; Xie et al. 2024). However, its massive data volume imposes significant challenges on storage and transmission, hindering widespread adoption. Compared to pixelized 2D images and videos, DPC features more flexible geometry, making spatial and temporal dependencies harder to model.

Most existing DPC compression methods perform inter-prediction on consecutive frames using hand-crafted temporal context selection algorithms. The method in (Santos et al. 2021) employs various point cloud partitioning and matching strategies to identify correspondences between regions.

Copyright © 2026, Association for the Advancement of Artificial Intelligence (www.aaai.org). All rights reserved.

A motion-compensated approach for encoding dynamic voxelized point clouds at low bit rates is also proposed in (De and Chou 2017). Other methods rely on projection-based algorithms (Zhu et al. 2020). Among these method, the Moving Picture Experts Group (MPEG) proposes Video-based Point Cloud Compression (V-PCC) (Schwarz et al. 2018), which projects DPC into 2D geometry and texture videos, and then leverages mature video codecs such as HEVC to compress the generated videos.

Inspired by the success of deep learning in image and video compression, numerous efforts have been devoted to neural point cloud compression. The core of compression lies in removing redundancy. In dynamic point cloud compression (DPCC), existing methods mainly tackle spatial and temporal redundancies. To reduce spatial redundancy, VAEs are employed to downsample and aggregate features into a latent space (Huang, Lazzarotto, and Ebrahimi 2024), which is then quantized and encoded using probabilistic models. For temporal redundancy, common approaches use motion estimation and KNN-based motion compensation in latent space (Fan et al. 2022; Xia et al. 2023). D-DPCC (Fan et al. 2022) uses 3DAWI, an explicit KNN-based motion estimation method, to estimate motion, predict the target frame, and encode the residual. Follow-up works (Xia et al. 2023; Jiang et al. 2023, 2025) aim to enhance motion accuracy to reduce residual bitrate. However, due to scale variation, non-uniform geometry, and inconsistent orientation, motion estimation in point clouds remains challenging, limiting the effectiveness of residual-based coding.

To enable more flexible motion modeling, this paper reformulates conventional motion estimation and compensation as a spatiotemporal alignment task. Specifically, a point-based alignment module is introduced to implicitly model dynamic variations, offering higher adaptability to local deformations compared to explicit motion models. Furthermore, a random access (RA) coding scheme is employed, which replaces sequential frame-by-frame encoding with a non-sequential hierarchical structure. This design improves compression efficiency and supports parallel encoding, enabling faster and more scalable processing.

The contributions of our work are as follows:

- To overcome the limitations of traditional motion estima-

tion in capturing local deformations, we propose a novel motion modeling approach by casting it as a spatiotemporal alignment task, implemented via feature-aligned motion Transformation (FMT) with MLPs.

- To address limitations of sequential encoding in temporal modeling, we propose a novel random access (RA) mode built upon a hierarchical non-sequential reference structure, enabling dynamic selection of forward and backward frames and improving compression efficiency.
- Experimental results confirm that the proposed method offers substantial gains in both encoding efficiency and compression performance over those representative baseline methods, such as D-DPCC and AdaDPCC.

Related Work

Dynamic Point Cloud Compression

Dynamic point cloud compression has been widely explored, with methods broadly categorized into rule-based and learning-based approaches. Rule-based methods, such as the MPEG V-PCC standard (Schwarz et al. 2018), project 3D point clouds onto 2D planes and compress them using traditional video codecs (Li et al. 2019). Other techniques, including PatchVVC (Chen et al. 2023) and the framework by Mekuria et al. (Mekuria, Blom, and Cesar 2016), reduce inter-frame redundancy in 3D space through block or patch matching. However, these methods rely on explicit motion estimation, which often struggles to capture localized movements in large-scale, dense point clouds, especially under non-uniform distributions or scale variations.

Learning-based methods have demonstrated superior performance in both static and dynamic point cloud compression (Wang et al. 2022; Zhang et al. 2023; Wang et al. 2024, 2021). For static point clouds (Fu et al. 2022; Cui et al. 2023; Nguyen and Kaup 2023), these approaches mainly focus on reducing spatial redundancy in coordinate data. For dynamic point clouds, temporal redundancy is addressed through inter-frame prediction, often via temporal convolutions. Akhtar et al. (Akhtar, Li, and Van der Auwera 2024) propose a geometry compression predictor that compensates the current frame’s latent representation using reference neighbors. Unicorn (Wang et al. 2024) adopts a unified framework combining context modeling and multiscale motion compensation. More advanced techniques, such as D-DPCC (Fan et al. 2022) with end-to-end learned motion estimation, and Xia et al.’s (Xia et al. 2023) two-layer coarse-to-fine compensation, enhance temporal prediction. Jiang et al. (Jiang et al. 2023) further introduce multiscale motion estimation by using coarse motion as a prior for finer-scale refinement, while MP-VPC (Jiang et al. 2025) incorporates a feature proxy module to adaptively locate representative points for motion modeling.

Despite these advances, existing methods typically adopt a sequential pipeline consisting of explicit motion estimation, motion compensation, and residual encoding. However, such approaches often struggle to effectively capture subtle yet localized deformations in real-world dynamic point clouds, thereby limiting their adaptability to complex and diverse scenarios. In contrast, our work addresses these chal-

lenges by reformulating motion modeling as a spatiotemporal alignment task, where the proposed Feature-aligned Motion Transformation (FMT) implicitly captures temporal variations without relying on explicit motion estimation. Furthermore, the proposed non-sequential hierarchical encoding paradigm dynamically selects both forward and backward reference frames, enabling more flexible temporal context modeling and improved compression efficiency.

Point Cloud Scene Flow Estimation

Scene flow estimation extends 2D optical flow to 3D point clouds, enabling motion vector (MV) estimation in three-dimensional space. FlowNet3D (Liu, Qi, and Guibas 2019) leverages PointNet++ (Qi et al. 2017) for feature extraction and fusion, while PointPWC-Net (Wu et al. 2020) adopts a coarse-to-fine strategy with cost volumes. Pv-Raft (Wei et al. 2021) introduces point-voxel correlation fields to capture both local and long-range point dependencies. Although effective, these methods are computationally expensive on large, dense point clouds due to their high dimensionality.

In large-scale sequences, motion is subtle but significant in localized areas, where existing methods struggle with heterogeneous patterns due to non-uniform distributions. Our framework redefines motion modeling as a spatiotemporal alignment task, using implicit neural representations via MLPs. We introduce a latent space feature prediction module, anchoring current frame coordinates and using KNN (Wu, Qi, and Fuxin 2019) to correlate reference features, predicting current frame features without 3D flow vectors, enhancing adaptability to localized deformations.

Learned Video Compression

Learned video compression has inspired dynamic point cloud compression (Hu, Lu, and Xu 2021; Hu et al. 2022; Lu et al. 2019). AI-based codecs like DVC (Lu et al. 2019) and FVC (Hu, Lu, and Xu 2021) perform motion estimation and compensation in pixel or feature domains, encoding residuals between warped references and current frames. Context-based frameworks further enhance temporal prediction by leveraging motion-compensated features (Li, Li, and Lu 2021, 2023, 2024). However, due to point clouds’ irregular geometry and complex motion, such methods struggle with non-uniform distributions and diverse motion patterns.

Methodology

Overview

The overall compression framework is shown in Figure 1. At the encoder side, the input point cloud is progressively downsampled, and the resultant coordinates are losslessly compressed using a hybrid codec based on entropy coding and octree representation. The coordinates of the current frame and bidirectional references are then aligned via the FMT module to produce latent features, which serve as spatiotemporal context for the Conditional Entropy Model. At the decoder side, point clouds are reconstructed from the bit-stream following the RA coding order, with decoded frames buffered as future references.

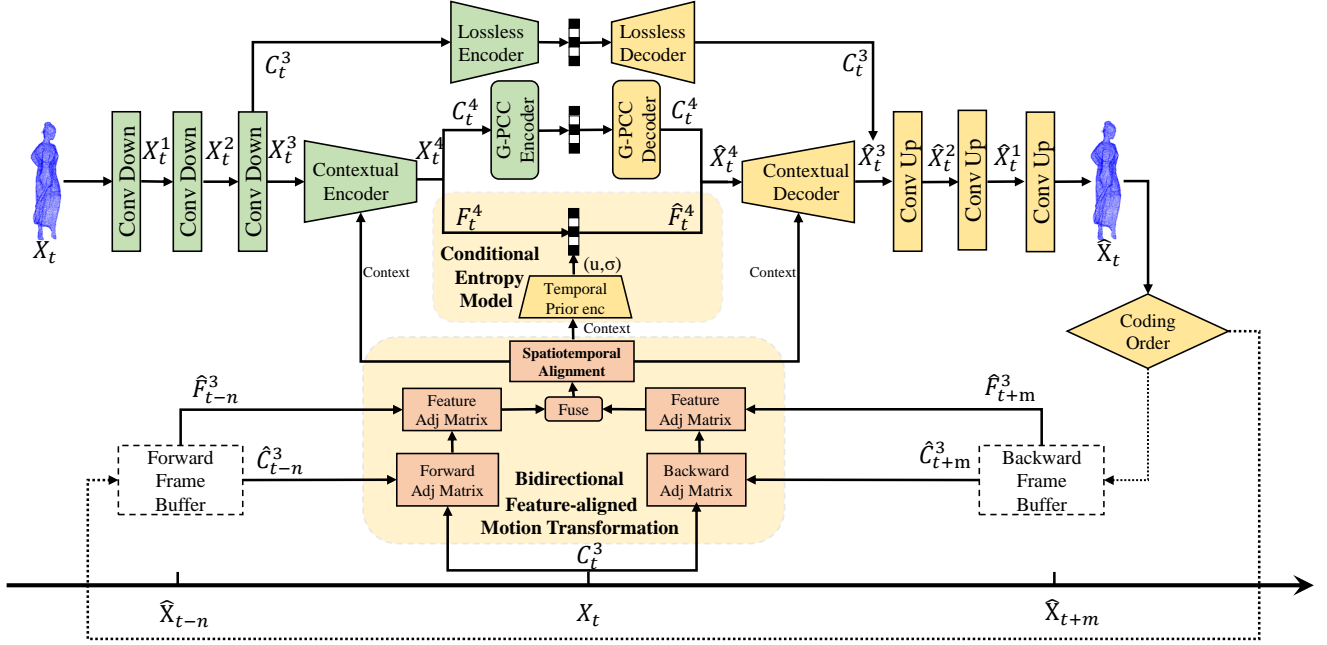


Figure 1: The framework employs a non-sequential hierarchical encoding mode. The input point cloud X_t is downsampled via three sparse convolutions to produce X_t^3 , consisting of coordinates C_t^3 and features F_t^3 . These are processed with reference frames at $t-n$ and $t+m$ through a Bidirectional Implicit Neural Motion Representation module to generate temporally spatiotemporally aligned features, which serve as temporal context for latent feature modeling. The Contextual Encoder compresses C_t^4 via Octree encoding, while F_t^4 is compressed in a lossy manner and subsequently reconstructed as \hat{F}_t^4 . The Contextual Decoder takes C_t^3 and $F_t^{3\text{aligned}}$ as input and reconstructs the point cloud \hat{X}_t^3 , which is then decoded to \hat{X}_t . The decoded point cloud is stored in either the forward or backward frame buffer.

Encoding pipeline. At time t , the input point cloud is denoted as $X_t = \{(C_t, F_t)\}$, where $C_t \in \mathbb{R}^{N \times 3}$ are the coordinates and $F_t \in \mathbb{R}^{N \times d}$ are the associated features. The point cloud is progressively downsampled through three Downsampling Blocks, yielding X_t^1 , X_t^2 , and X_t^3 , with $X_t^k = (C_t^k, F_t^k)$ denoting the stage- k latent representation of frame t .

The downsampled coordinates C_t^3 , together with reference frames $\{X_{t-n}, X_{t+m}\}$ stored in the buffer, are fed into the Bidirectional Feature-aligned Motion Transformation (Bi-FMT) module, which aligns the reference features to the current frame and outputs the motion-aware context $F_t^{3\text{aligned}}$. The concatenation of X_t^3 and $F_t^{3\text{aligned}}$ is then encoded by the Contextual Encoder, producing a higher-level latent representation $X_t^4 = (C_t^4, F_t^4)$.

For compression, different strategies are adopted for different coordinate levels: (i) F_t^4 is compressed by the Conditional Entropy Model; (ii) C_t^4 is losslessly encoded by the octree-based G-PCC geometry codec; (iii) C_t^3 is compressed by a learned end-to-end lossless geometry codec (similar to DDPC (Fan et al. 2022)) to preserve the structural details required for alignment at the decoder side.

Decoding pipeline. At the decoder side, C_t^3 is first recovered from the learned lossless codec, while C_t^4 is reconstructed by the G-PCC octree decoder. The latent features \hat{F}_t^4 are simultaneously obtained from the entropy de-

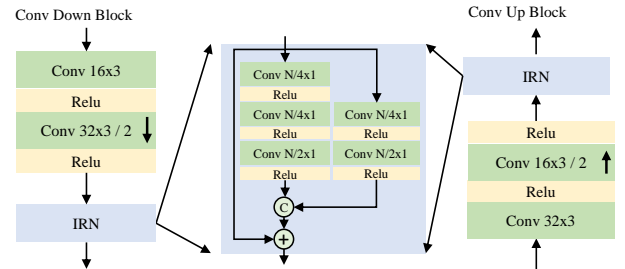


Figure 2: Architectural details of the upsampling and downsampling modules.

coder, leading to the high-level latent representation $\hat{X}_t^4 = (C_t^4, \hat{F}_t^4)$.

The Bi-FMT module then aligns the reference features using the decoded coordinates to reconstruct the context $F_t^{3\text{aligned}}$. Both \hat{F}_t^4 from \hat{X}_t^4 and $F_t^{3\text{aligned}}$ are incorporated by the Contextual Decoder, which generates the temporally aligned features \hat{F}_t^3 . Combining \hat{F}_t^3 with C_t^3 forms the latent point cloud $\hat{X}_t^3 = (C_t^3, \hat{F}_t^3)$. Finally, \hat{X}_t^3 is progressively upsampled to obtain \hat{X}_t^2 , \hat{X}_t^1 , and the full-resolution reconstruction \hat{X}_t , which is stored in the reference buffer according to the RA coding order.

Algorithm 1: Algorithm 1: Feature-aligned Motion Transformation

Input: point cloud $X_t = \{x_i^t\}_{i=1}^{N_{origin}}$, reference point cloud $X_{t-n} = \{x_j^{t-n}\}_{j=1}^{M_{origin}}$

Steps:

- 1: Downsample X_t and X_{t-n} to obtain coordinate sets $C_t = \{c_i^t\}_{i=1}^N$, $C_{t-n} = \{c_j^{t-n}\}_{j=1}^M$.
- 2: **for** each $c_i^t \in C_t$ **do**
- 3: Find K nearest neighbors in C_{t-n} : $\mathcal{N}_i = \{c_{j_k}^{t-n} \mid j_k = \arg \min_j \|c_i^t - c_j^{t-n}\|, k = 1, \dots, K\}$, then get a fixed adjacency matrix $\text{Adj} \in \mathbb{R}^{N \times K \times 3}$.
- 4: Extract neighbor features $F_{\mathcal{N}_i} = \{f_{j_k}^{t-n}\}_{k=1}^K$ and compute relative coordinates: $\Delta x_i = \{c_i^t - c_{j_k}^{t-n}\}_{k=1}^K$.
- 5: Concatenate feature and relative coordinates $H_i = \text{concat}(F_{\mathcal{N}_i}, \Delta x_i) \in \mathbb{R}^{K \times (C+3)}$, then compute softmax via $\alpha_i = \text{Softmax}(\text{MLP}(H_i)) \in \mathbb{R}^{K \times 1}$ and modulate neighbor features by $\tilde{F}_{\mathcal{N}_i} = \alpha_i \odot F_{\mathcal{N}_i}$.
- 6: Concatenate modulated features and anchor coordinate: $Z_i = \text{concat}(\tilde{F}_{\mathcal{N}_i}, x_i) \in \mathbb{R}^{K \times (C+3)}$.
- 7: Apply MLP Networks on Z_i to predict feature for point x_i : $f_{aligned} = \text{MLP}(Z_i) \in \mathbb{R}^C$, and then collect all predicted features: $F_{aligned} = \{f_{aligned}\}_{i=1}^N \in \mathbb{R}^{N \times C}$.
- 8: **end for**

Output: predicted features $F_{aligned}$ for X_t

Upsampling and Downsampling Modules. Figure 2 illustrates the architecture of the point cloud downsampling and upsampling modules. ‘Conv $c \times n$ ’ denotes a sparse convolution operation with c output channels and a kernel size of $n \times n \times n$, implemented using the MinkowskiEngine (ME) library. ‘ $s \uparrow$ ’ and ‘ $s \downarrow$ ’ represent upsampling and downsampling operations with a factor of s , respectively. ‘ReLU’ refers to the Rectified Linear Unit, and ‘IRN’ denotes the Inception-Residual Network, which is employed for efficient feature aggregation.

Specifically, The Contextual Encoder builds upon the downsampling block by integrating the input feature X_t^3 with contextual information, producing enhanced features that capture both local and contextual cues. Likewise, the Contextual Decoder extends the upsampling block by fusing the reconstructed feature \hat{X}_t^4 with contextual information, enabling more accurate feature reconstruction. The Contextual Encoder and Decoder can be formally expressed as

$$\begin{aligned} f_{CE}(X_t^3, \text{Context}) &= \text{DownBlock}(X_t^3) + \Phi(\text{Context}), \\ f_{CD}(\hat{X}_t^4, \text{Context}) &= \text{UpBlock}(\hat{X}_t^4) + \Phi(\text{Context}), \end{aligned} \quad (1)$$

where Φ denotes the operation that integrates contextual information into the feature blocks.

Feature-aligned Motion Transformation

In dynamic point cloud compression, modeling spatiotemporal correlations between reference and target frames is essential for effective inter-frame prediction. Due to the irregu-

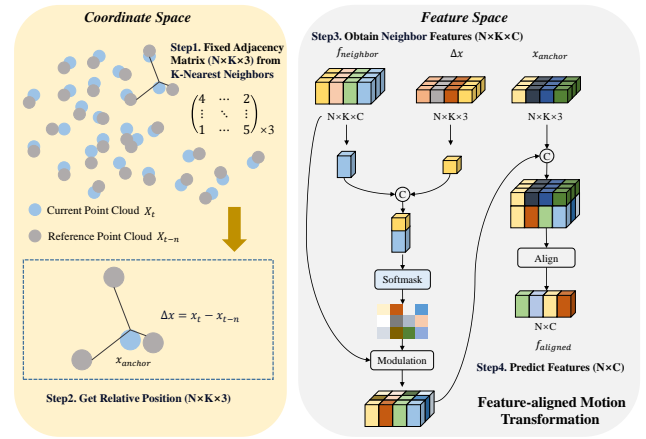


Figure 3: Detailed Illustration of the Implicit Neural Motion Representation for Spatiotemporal Alignment.

lar and unordered nature of point clouds, explicit point-wise motion estimation is often unreliable and computationally unstable. Previous methods typically rely on iterative motion refinement, where the KNN adjacency matrix is updated at each step. However, this continual change in neighborhood structure introduces significant variability, making the motion training process unstable and increasing the difficulty of learning accurate motion fields. To mitigate these challenges, we reformulate the spatiotemporal alignment task as a feature alignment problem. Specifically, a fixed KNN graph is established for each point in the current frame, which is then employed to aggregate point features in the reference frame. The aggregated features are subsequently aligned via a lightweight MLP to produce a motion-aware temporal context for conditional encoding. This approach circumvents explicit motion estimation and maintains structural consistency during training.

Our proposed framework eliminates the need for transmitting motion-related bitstreams. Instead, the motion of dynamic point clouds is modeled through a Feature-aligned Motion Transformation (FMT) module at both the encoding and decoding stages. Specifically, KNN-based correspondence between X_t and X_{t-n} is first established to extract neighbor features and relative offsets, which are then interpolated and dynamically aligned via a lightweight MLP to produce motion-aware temporal context for encoding, entropy modeling, and reconstruction. Compared with AuxGR (Liu et al. 2024), which employs KNN with self-attention to flexibly capture temporal correlations under large motions, FMT ensures structural consistency of the KNN graph and improves training stability by adopting a feature alignment-driven design.

Conditional Entropy Model

We use the factorized entropy model for hyper prior and Laplace distribution to model the latent representations as (Li, Li, and Lu 2021). According to (Shannon 1948), the cross-entropy between the estimated probability distribution and the actual latent code distribution is a tight lower bound

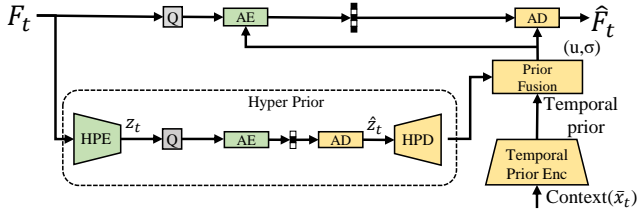


Figure 4: Our entropy model used to encode the quantized latent codes \hat{F}_t . HPE and HPD are hyper prior encoder and decoder. Q means quantization. AE and AD are arithmetic encoder and decoder.

of the actual bitrate, namely

$$R(\hat{y}_t) = \mathbb{E}_{\hat{y}_t \sim q_{\hat{y}_t}} [\log_2 p_{\hat{y}_t}(\hat{y}_t)], \quad (2)$$

where $p_{\hat{y}_t}(\hat{y}_t)$ and $q_{\hat{y}_t}(\hat{y}_t)$ denote the estimated and the true probability mass functions of the quantized latent codes \hat{y}_t , respectively. The gap between the actual bitrate $R(\hat{y}_t)$ and the bitrate estimated by cross-entropy is negligible. Therefore, our objective is to design an entropy model that can accurately estimate the probability distribution $p_{\hat{y}_t}(\hat{y}_t)$ of the latent codes. The framework of our entropy model is illustrated in Figure 4. First, we use the hyper prior model (Ballé et al. 2018) to learn the hierarchical prior and use autoregressive network (Minnen, Ballé, and Toderici 2018) to learn the spatial prior. Meanwhile, we design a temporal prior encoder to explore the temporal correlation. The prior fusion network is trained to fuse three different priors and estimate the mean and scale of the latent code distribution. In this paper, we follow the existing work (Kamisli, Racapé, and Choi 2024) and assume that $p_{\hat{F}_t}(\hat{F}_t)$ follows the Laplace distribution:

$$p_{\hat{F}_t}(\hat{F}_t | \bar{x}_t, \hat{z}_t) = \prod_i \mathcal{L}(\mu_i, \sigma_i) \cdot \mathcal{U}\left(-\frac{1}{2}, \frac{1}{2}\right)(\hat{F}_{t,i}), \quad (3)$$

where

$$\mu_i, \sigma_i = f_{\text{pf}}\left(f_{\text{hpd}}(\hat{z}_t), f_{\text{ar}}(\hat{F}_{t,<i}), f_{\text{tpe}}(\bar{x}_t)\right). \quad (4)$$

The index i represents the spatial location. $f_{\text{hpd}}(\cdot)$ denotes the hyper prior decoder network, $f_{\text{ar}}(\cdot)$ is the autoregressive network, and $f_{\text{tpe}}(\cdot)$ refers to the specially designed temporal prior encoder network. $f_{\text{pf}}(\cdot)$ denotes the prior fusion network, the context \bar{x}_t is to generate the temporal prior.

In our entropy model, $f_{\text{ar}}(\hat{F}_{t,<i})$ and $f_{\text{tpe}}(\bar{x}_t)$ provide the spatial and temporal priors, respectively, while $f_{\text{hpd}}(\hat{z}_t)$ provides the supplemental side information that cannot be learned from spatial or temporal correlations.

Random Access (RA) Reference Strategy

To boost the proposed FMT framework, a non-sequential, hierarchical Group of Frames (GOF) structure is designed to further enhance temporal modeling and compression efficiency. Unlike conventional video codecs that periodically insert I-frames to mitigate drift, dynamic point cloud sequences exhibit stable coding quality across long durations.

Thus, only the first frame in the entire sequence is intra-coded, while all subsequent frames are inter-coded.

Following the open-GOF configuration inspired by H.266 (Bross et al. 2021), each GOF consists of 16 frames organized into five hierarchical layers and is encoded in a bottom-up, layer-wise manner. To maintain temporal continuity, the first frame of each GOF references the last frame of the preceding GOF, employing inter-frame coding. All frames are encoded in a non-sequential order to maximize temporal prediction efficiency, following the coding order in a GOF (i.e., 0, 8, 4, 12, 2, 6, 10, 14, 1, 3, 5, 7, 9, 11, 13, 15), as illustrated in Figure 5. Since the reference frames for higher-layer frames are exclusively located in lower layers, frames within the same layer can be encoded and decoded in parallel, enabling efficient synchronization across the hierarchy (Sullivan et al. 2012).

Within each GOF, both unidirectional and bidirectional predictions are employed with precision based on spatiotemporal relevance. For instance, Frame 14 uses Frame 12 as its primary single reference due to its proximity, while Frame 10 utilizes bidirectional cues from Frames 8 and 12 for significantly enhanced prediction.

Loss Function

Given an input point cloud x , the optimization objective of the network is shown in Equation 5, where λ is the Lagrange multiplier that controls the trade-off between bitrate and distortion. Here, $f(\cdot)$ and $g(\cdot)$ denote the encoder and decoder, respectively, and quantization is denoted by $[\cdot]$:

$$\mathbb{E}_{x \sim p_x} [-\log p_y([f(x)])] + \lambda \cdot \mathbb{E}_{x \sim p_x} [d(x, g([f(x)]))] \quad (5)$$

As described in Equation 5, the loss function is modeled as a joint optimization of rate and distortion, i.e., $R + \lambda \cdot D$. Since z_t serves as side information, its bitrate must also be included in the total rate calculation. Accordingly, the estimated rate is given by Equation 6, while the distortion is computed using the Binary Cross Entropy (BCE) loss, following PCGCv2 (Bross et al. 2021), as shown in Equation 7:

$$R = \mathbb{E}_{x \sim p_x} \left[\sum_t (\log p(y_t | y_{t-1}, z_t) + \log p(z_t)) \right] \quad (6)$$

$$D = \frac{1}{K} \sum_{k=1}^K \left(\frac{1}{N_k} \sum_v - (O_v \log p_v + (1 - O_v) \log(1 - p_v)) \right) \quad (7)$$

In Equation 7, O_v denotes the ground-truth occupancy value for voxel v , p_v is the predicted occupancy probability, and N_k is the number of voxels considered at the k -th upsampling stage. To minimize distortion, BCE losses from all K stages of the synthesis transform are averaged, yielding the final distortion metric.

Experiments

Implementation Details

Training Dataset. We train our model using the OwlII dataset (Yi Xu and Wen 2017), which comprises four se-

Dataset	Gain over V-PCC		Gain over D-DPCC		Gain over PatchDPCC		Gain over AdaDPCC		Gain over PCGCv2	
	D1 (%)	D2 (%)	D1 (%)	D2 (%)	D1 (%)	D2 (%)	D1 (%)	D2 (%)	D1 (%)	D2 (%)
Longdress	-68.24	-70.81	-23.58	-24.67	-19.18	-46.96	-13.95	-17.60	-43.43	-60.92
Loot	-70.07	-90.63	-22.45	-21.41	-17.18	-32.07	-9.55	-7.70	-49.08	-60.03
Redandblack	-75.56	-96.75	-15.44	-20.22	-9.52	-48.44	-8.96	-20.91	-36.70	-63.55
Soldier	-86.12	-98.26	-19.14	-16.66	-8.87	-38.36	-5.15	-4.01	-52.78	-58.81
Average	-75.00	-89.11	-20.15	-20.74	-13.69	-41.46	-9.40	-12.55	-45.5	-60.83

Table 1: BD-Rate gains measured using both D1 PSNR(%) and D2 PSNR(%) for IMNR-DPCC (ours) against the V-PCC, D-DPCC (Fan et al. 2022, IJCAI), PatchDPCC (Pan et al. 2024, AAAI), AdaDPCC (Zhang et al. 2025, AAAI) and PCGCv2 (Wang et al. 2021, DCC) for lossy coded point clouds. The larger the negative percentage, the greater the gain of our method.

Method	Soldier	Redandblack	Loot	Longdress	Average
Ours	0.63 / 0.57	0.50 / 0.52	0.62 / 0.58	0.62 / 0.61	0.59 / 0.57
D-DPCC	1.36 / 1.21	1.29 / 1.13	1.19 / 1.12	1.26 / 1.16	1.28 / 1.16
PatchDPCC	5.06 / 1.34	4.75 / 1.12	4.86 / 1.10	4.98 / 1.20	4.912 / 1.19
AdaDPCC	0.71 / 0.67	0.58 / 0.63	0.69 / 0.68	0.72 / 0.71	0.68 / 0.67

Table 2: Average coding time comparison (encoding / decoding) on the 8iVFB dataset. Time is measured in seconds (s).

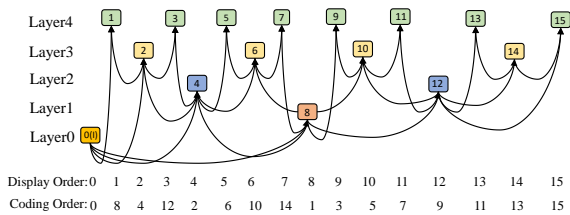


Figure 5: Illustration of the hierarchical RA referencing structure for a GoF of 16. Frames are organized into five temporal layers and encoded in non-sequential order. Arrows indicate reference dependencies. Layer 0 (yellow) is the I-frame, while other frames serve as P/B references according to their layer. This strategy enables bidirectional prediction, random access, and efficient parallel encoding.

quences with totally 2400 frames, with each sequence lasting 20 seconds at 30 frames per second (FPS). To optimize training efficiency, we quantize the original 11-bit precision point cloud data to 10-bit.

Evaluation Dataset. Following the MPEG common test condition (CTC) (mpe 2021), we evaluate the performance of the proposed D-DPCC framework using 8i Voxelized Full Bodies (8iVFB) (d’Eon et al. 2017), containing 4 sequences with 1200 frames. The frame rate is 30 fps over 10 seconds. We adhere to the MPEG common test condition (CTC), setting the GoF size to 16. The first frame of each GoF is designated as an “I” frame and encoded by SparsePCC (Wang et al. 2022) while subsequent frames are labeled as “P” frames or “B” frames and encoded by the proposed method. In the coding structure, “P” denotes uni-directional reference, and “B” denotes bi-directional reference.

Implementation Details. We train FMT-DPCC with $\lambda = \{1, 3, 5, 8\}$ for each rate point. We utilize an Adam (Kinga, Adam et al. 2015) optimizer with $\beta = (0.9, 0.999)$, together with a learning rate scheduler with a decay rate of 0.5 for every 15 epochs. A two-stage training strategy is applied for each rate point. Specifically, for the first five epochs, λ is set as 30 to accelerate the convergence of the point cloud reconstruction module. Then, the model is trained for another 45 epochs with λ set to its original value. The training is carried out on an NVIDIA A100 GPU with a batch size of 1.

Evaluation Metrics. The bit rate is evaluated using bits per point (bpp), and the distortion is evaluated using point-to-point geometry (D1) Peak Signal-to-Noise Ratio (PSNR) and point-to-plane geometry (D2) PSNR following the MPEG CTC. The peak value p is set as 1023 for 8iVFB.

Experimental Results

Baseline Setup

We compare the proposed FMT-DPCC with the current state-of-the-art dynamic point cloud geometry compression framework: V-PCC Test Model v13, using quantization parameter (QP) settings of 18, 15, 12, 10, and 8, respectively. We also conducted a comparison with existing deep learning-based frameworks for dynamic point cloud geometry compression, including D-DPCC (Fan et al. 2022), patchDPCC (Pan et al. 2024), and AdaDPCC (Zhang and Gao 2025). Furthermore, we included a comparison with PCGCv2 (Wang et al. 2021), which is commonly employed for static point cloud compression.

Performance Evaluation

Quantitative comparison. The rate-distortion curves achieved by methods are depicted in Figure 6, with the corresponding BD-Rate gains summarized in Table 1. Com-

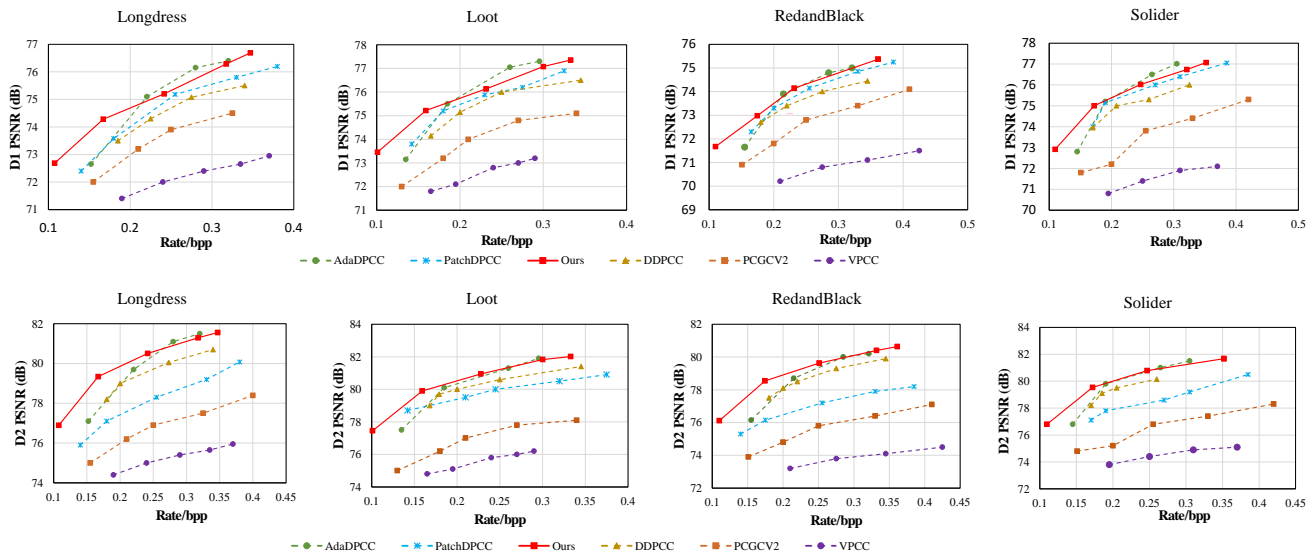


Figure 6: D1-PSNR and D2-PSNR Rate-distortion curves of different compression methods on MPEG 8i.

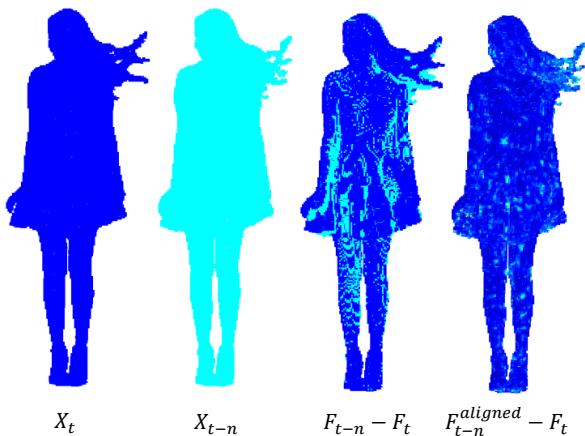


Figure 7: From left to right: point cloud at time t , reference point cloud at time $t-n$, feature difference before alignment, and reduced feature difference after alignment.

pared with the projection-based method like V-PCC, the proposed method targets 3D space compression with powerful learning-based modules and culminates in BD-Rate reduction exceeding 75.00% (D1) and 89.11% (D2) on average. Furthermore, our method achieves an average BD-Rate reduction relative to PCGCV2 exceeding 45.5% for D1 and 60.83% for D2. Compared with other learning-based dynamic point cloud compression approaches (Fan et al. 2022; Pan et al. 2024; Zhang and Gao 2025), our framework demonstrates superior performance, particularly in terms of the D2-PSNR metric.

It is worth noting that the performance gains over AdaDPCC become more prominent under low bitrate scenarios. This can be attributed to the global effectiveness of the

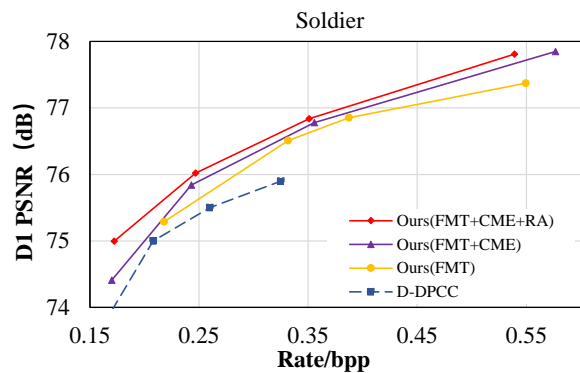


Figure 8: Ablation study on RD performance. The contributions of major components are evaluated: FMT (Feature-aligned Motion Transformation) models motion implicitly, CME (Conditional Entropy Model) improves compression with learned priors, and RA (Random Access) enables hierarchical non-sequential coding.

implicit alignment process, which is particularly beneficial when bit resources are constrained, enabling more efficient representation of temporal dynamics.

Coding time comparison. Table 2 presents a comprehensive comparison of average encoding and decoding times on the 8iVFB dataset. Our method demonstrates a significant advantage in both encoding and decoding efficiency over existing approaches. Specifically, our framework achieves an encoding time of 0.59s, which is $1.15\times$ faster than AdaDPCC (0.68s) and $8.32\times$ faster than PatchDPCC (4.91s). For decoding, our method requires only 0.57s, achieving $1.18\times$ speedup over AdaDPCC (0.67s) and $2.09\times$ speedup over PatchDPCC (1.19s). Note that V-PCC involves a projection

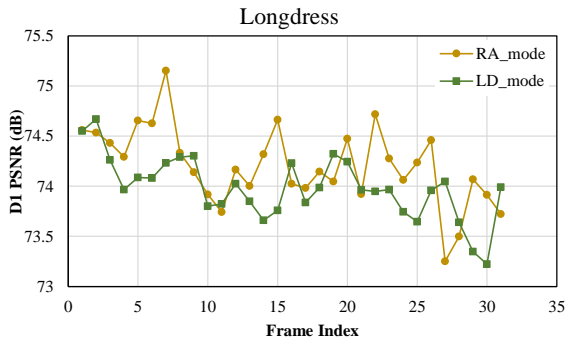


Figure 9: Quality fluctuation analysis on the Longdress sequence under both non-sequential (RA) and sequential (LD) coding modes.

process from 3D data to 2D and is executed primarily on CPUs, resulting in extremely long encoding times, therefore, it is not included in the comparison.

These results highlight the substantial runtime efficiency of our proposed method. The significant reduction in both encoding and decoding latency makes it particularly suitable for real-time or resource-constrained applications.

It is worth noting that our current implementation does not yet incorporate parallel acceleration based on the hierarchical reference structure. Since the hierarchical reference structure is inherently well-suited for parallel processing, we expect that both encoding and decoding speeds can be further improved with parallelization (Sullivan et al. 2012).

Ablation Study

RD performance. To validate the effectiveness of our proposed modules, including the FMT module, the Conditional Entropy Model (CEM) based on FMT, and the unordered hierarchical coding structure under the Random Access (RA) mode, we conducted extensive ablation studies.

The ablation results, presented in Figure 8, are obtained on the *Soldier* sequence. By progressively removing each module, we observed a consistent degradation in RD performance, demonstrating the importance of each component. The FMT module alone provides a significant improvement, achieving a BD-Rate reduction of approximately 10.86% compared to the 3DAWI method in D-DPCC. 3DAWI is an explicit KNN-based motion estimation method. By leveraging the FMT-aligned features as context and integrating them with the hyperprior to construct a hyperprior-context model, we achieve an additional BD-Rate gain of approximately 7.41%. Furthermore, integrating the unordered hierarchical reference structure under the Random Access configuration yields a further BD-Rate reduction of approximately 5.07%. These results highlight the effectiveness and synergy of our framework components. To demonstrate the effectiveness of the FMT-based spatiotemporal alignment, we visualize the feature errors with respect to the target before and after alignment. As shown in Figure 7, the unaligned reference features F_{t-n} differ significantly from the current features, while the aligned features F_{t-n}^{aligned} exhibit

noticeably reduced errors, with smaller high-error regions.

Random Access (RA) Reference Strategy. Under the random access (RA) mode, dynamic point clouds are divided into fixed-length groups of frames (GOFs) and encoded following a predefined hierarchical structure, where higher-layer frames can reference both past and future frames for bidirectional prediction. Figure 9 illustrates the quality fluctuations in two consecutive GOFs under both RA and sequential low-delay (LD) modes. Benefiting from bidirectional referencing, frames in the RA mode generally achieve noticeably higher quality compared to those in the LD mode, which relies solely on unidirectional prediction. However, the larger temporal gaps in RA may introduce less relevant or noisier features, causing a few frames (e.g., the 1st, 9th, and 16th) to exhibit slightly lower quality than their LD counterparts, which always reference the nearest past frame. Overall, the observed quality trends clearly demonstrate that the hierarchical RA strategy significantly improves dynamic point cloud compression by enhancing rate-distortion performance and enabling frame-level parallel encoding, making it suitable for real-time applications.

Conclusion

This paper proposes a novel deep compression framework for dynamic point clouds based on Implicit Neural Motion Representation. By leveraging spatiotemporal alignment to capture continuous geometric variations, the method circumvents explicit motion estimation and effectively models temporal dependencies within a latent-space conditional coding structure. Furthermore, a random access hierarchical reference strategy is introduced to enable bidirectional motion referencing and frame-level parallelism, thereby enhancing both flexibility and compression efficiency. Extensive experiments demonstrate that the proposed framework achieves state-of-the-art performance in terms of rate-distortion trade-off and computational efficiency.

References

2021. ISO/IEC 23090-12:2021 Information technology — Coded representation of immersive media — Part 12: MPEG Point Cloud Compression (MPEG-PCC).
- Akhtar, A.; Li, Z.; and Van der Auwera, G. 2024. Inter-frame compression for dynamic point cloud geometry coding. *IEEE Transactions on Image Processing*, 33: 584–594.
- Ballé, J.; Minnen, D.; Singh, S.; Hwang, S. J.; and Johnston, N. 2018. Variational image compression with a scale hyperprior. *arXiv preprint arXiv:1802.01436*.
- Bross, B.; Wang, Y.-K.; Ye, Y.; Liu, S.; Chen, J.; Sullivan, G. J.; and Ohm, J.-R. 2021. Overview of the versatile video coding (VVC) standard and its applications. *IEEE Transactions on Circuits and Systems for Video Technology*, 31(10): 3736–3764.
- Chen, R.; Xiao, M.; Yu, D.; Zhang, G.; and Liu, Y. 2023. patchVVC: A real-time compression framework for streaming volumetric videos. In *Proceedings of the 14th Conference on ACM Multimedia Systems*, 119–129.

- Cui, M.; Long, J.; Feng, M.; Li, B.; and Kai, H. 2023. OctFormer: Efficient octree-based transformer for point cloud compression with local enhancement. In *Proceedings of the AAAI Conference on Artificial Intelligence*, volume 37, 470–478.
- De, R.; and Chou, P. A. 2017. Motion-compensated compression of dynamic voxelized point clouds. *IEEE Transactions on Image Processing*, 26(8): 3886–3895.
- d’Eon, E.; Harrison, B.; Myers, T.; and Chou, P. A. 2017. 8i voxelized full bodies—a voxelized point cloud dataset. *ISO/IEC JTC1/SC29 Joint WG11/WG1 (MPEG/JPEG) input document WG11M40059/WG1M74006*, 7(8): 11.
- Fan, T.; Gao, L.; Xu, Y.; Li, Z.; and Wang, D. 2022. D-dpcc: Deep dynamic point cloud compression via 3d motion prediction. *arXiv preprint arXiv:2205.01135*.
- Fu, C.; Li, G.; Song, R.; Gao, W.; and Liu, S. 2022. Octattention: Octree-based large-scale contexts model for point cloud compression. In *Proceedings of the AAAI conference on artificial intelligence*, volume 36, 625–633.
- Hu, Z.; Lu, G.; Guo, J.; Liu, S.; Jiang, W.; and Xu, D. 2022. Coarse-to-fine deep video coding with hyperprior-guided mode prediction. In *Proceedings of the IEEE/CVF Conference on Computer Vision and Pattern Recognition*, 5921–5930.
- Hu, Z.; Lu, G.; and Xu, D. 2021. FVC: A new framework towards deep video compression in feature space. In *Proceedings of the IEEE/CVF conference on computer vision and pattern recognition*, 1502–1511.
- Huang, B.; Lazzarotto, D.; and Ebrahimi, T. 2024. Temporal Conditional Coding for Dynamic Point Cloud Geometry Compression. In *ICASSP 2024-2024 IEEE International Conference on Acoustics, Speech and Signal Processing (ICASSP)*, 7920–7924. IEEE.
- Jiang, Z.; Han, D.; Song, C.; Nan, F.; and Yang, B. 2025. MP-DPCC: A Motion Proxy-Based Dynamic Point Cloud Compression Framework. In *ICASSP 2025-2025 IEEE International Conference on Acoustics, Speech and Signal Processing (ICASSP)*, 1–5. IEEE.
- Jiang, Z.; Wang, G.; Tam, G. K.; Song, C.; Li, F. W.; and Yang, B. 2023. An end-to-end dynamic point cloud geometry compression in latent space. *Displays*, 80: 102528.
- Kamisli, F.; Racapé, F.; and Choi, H. 2024. Variable-Rate Learned Image Compression with Multi-Objective Optimization and Quantization-Reconstruction Offsets.
- Kinga, D.; Adam, J. B.; et al. 2015. A method for stochastic optimization. In *International conference on learning representations (ICLR)*, volume 5. California;.
- Li, J.; Li, B.; and Lu, Y. 2021. Deep contextual video compression. *Advances in Neural Information Processing Systems*, 34: 18114–18125.
- Li, J.; Li, B.; and Lu, Y. 2023. Neural video compression with diverse contexts. In *Proceedings of the IEEE/CVF conference on computer vision and pattern recognition*, 22616–22626.
- Li, J.; Li, B.; and Lu, Y. 2024. Neural video compression with feature modulation. In *Proceedings of the IEEE/CVF Conference on Computer Vision and Pattern Recognition*, 26099–26108.
- Li, L.; Li, Z.; Zakharchenko, V.; Chen, J.; and Li, H. 2019. Advanced 3D motion prediction for video-based dynamic point cloud compression. *IEEE Transactions on Image Processing*, 29: 289–302.
- Liu, G.; Zhu, J.; Ding, D.; and Ma, Z. 2024. Encoding auxiliary information to restore compressed point cloud geometry. In *Proceedings of the Thirty-Third International Joint Conference on Artificial Intelligence, IJCAI-24*, 2189–2197.
- Liu, X.; Qi, C. R.; and Guibas, L. J. 2019. FlowNet3d: Learning scene flow in 3d point clouds. In *Proceedings of the IEEE/CVF conference on computer vision and pattern recognition*, 529–537.
- Lu, G.; Ouyang, W.; Xu, D.; Zhang, X.; Cai, C.; and Gao, Z. 2019. Dvc: An end-to-end deep video compression framework. In *Proceedings of the IEEE/CVF conference on computer vision and pattern recognition*, 11006–11015.
- Mekuria, R.; Blom, K.; and Cesar, P. 2016. Design, implementation, and evaluation of a point cloud codec for tele-immersive video. *IEEE Transactions on Circuits and Systems for Video Technology*, 27(4): 828–842.
- Minnen, D.; Ballé, J.; and Toderici, G. D. 2018. Joint autoregressive and hierarchical priors for learned image compression. *Advances in neural information processing systems*, 31.
- Nguyen, D. T.; and Kaup, A. 2023. Lossless point cloud geometry and attribute compression using a learned conditional probability model. *IEEE Transactions on Circuits and Systems for Video Technology*, 33(8): 4337–4348.
- Pan, Z.; Xiao, M.; Han, X.; Yu, D.; Zhang, G.; and Liu, Y. 2024. patchdpcc: A patchwise deep compression framework for dynamic point clouds. In *Proceedings of the AAAI Conference on Artificial Intelligence*, volume 38, 4406–4414.
- Qi, C. R.; Yi, L.; Su, H.; and Guibas, L. J. 2017. Pointnet++: Deep hierarchical feature learning on point sets in a metric space. *Advances in neural information processing systems*, 30.
- Santos, C.; Gonçalves, M.; Corrêa, G.; and Porto, M. 2021. Block-based inter-frame prediction for dynamic point cloud compression. In *2021 IEEE International Conference on Image Processing (ICIP)*, 3388–3392. IEEE.
- Schwarz, S.; Preda, M.; Baroncini, V.; Budagavi, M.; Cesar, P.; Chou, P. A.; Cohen, R. A.; Krivokuća, M.; Lasserre, S.; Li, Z.; et al. 2018. Emerging MPEG standards for point cloud compression. *IEEE Journal on Emerging and Selected Topics in Circuits and Systems*, 9(1): 133–148.
- Shannon, C. E. 1948. A mathematical theory of communication. *The Bell system technical journal*, 27(3): 379–423.
- Sullivan, G. J.; Ohm, J.-R.; Han, W.-J.; and Wiegand, T. 2012. Overview of the high efficiency video coding (HEVC) standard. *IEEE Transactions on circuits and systems for video technology*, 22(12): 1649–1668.
- Wang, J.; Ding, D.; Li, Z.; Feng, X.; Cao, C.; and Ma, Z. 2022. Sparse tensor-based multiscale representation for point cloud geometry compression. *IEEE Transactions on*

Pattern Analysis and Machine Intelligence, 45(7): 9055–9071.

Wang, J.; Ding, D.; Li, Z.; and Ma, Z. 2021. Multiscale point cloud geometry compression. In *2021 Data Compression Conference (DCC)*, 73–82. IEEE.

Wang, J.; Xue, R.; Li, J.; Ding, D.; Lin, Y.; and Ma, Z. 2024. A versatile point cloud compressor using universal multi-scale conditional coding–Part I: Geometry. *IEEE transactions on pattern analysis and machine intelligence*.

Wei, Y.; Wang, Z.; Rao, Y.; Lu, J.; and Zhou, J. 2021. Pv-raft: Point-voxel correlation fields for scene flow estimation of point clouds. In *Proceedings of the IEEE/CVF conference on computer vision and pattern recognition*, 6954–6963.

Wu, W.; Qi, Z.; and Fuxin, L. 2019. Pointconv: Deep convolutional networks on 3d point clouds. In *Proceedings of the IEEE/CVF Conference on computer vision and pattern recognition*, 9621–9630.

Wu, W.; Wang, Z. Y.; Li, Z.; Liu, W.; and Fuxin, L. 2020. Pointpwc-net: Cost volume on point clouds for (self-) supervised scene flow estimation. In *Computer Vision–ECCV 2020: 16th European Conference, Glasgow, UK, August 23–28, 2020, Proceedings, Part V 16*, 88–107. Springer.

Xia, S.; Fan, T.; Xu, Y.; Hwang, J.-N.; and Li, Z. 2023. Learning dynamic point cloud compression via hierarchical inter-frame block matching. In *Proceedings of the 31st ACM International Conference on Multimedia*, 7993–8003.

Xie, L.; Gao, W.; Zheng, H.; and Li, G. 2024. Roi-guided point cloud geometry compression towards human and machine vision. In *Proceedings of the 32nd ACM International Conference on Multimedia*, 3741–3750.

Xu, Y.; Zhang, K.; He, L.; Jiang, Z.; and Zhu, W. 2018. Introduction to point cloud compression. *ZTE Communications*, 16(3): 3.

Yi Xu, Y. L.; and Wen, Z. 2017. OwlII Dynamic Human Mesh Sequence Dataset. *ISO/IEC JTC1/SC29 Joint WG11/WG1 (MPEG/JPEG) input document WG11M40059/WG1M74006*, 7(8): 11.

Zhang, C.; and Gao, W. 2025. AdaDPCC: Adaptive Rate Control and Rate-Distortion-Complexity Optimization for Dynamic Point Cloud Compression. In *Proceedings of the AAAI Conference on Artificial Intelligence*, volume 39, 13188–13196.

Zhang, J.; Chen, T.; Ding, D.; and Ma, Z. 2023. YOGA: Yet another geometry-based point cloud compressor. In *Proceedings of the 31st ACM International Conference on Multimedia*, 9070–9081.

Zhu, W.; Ma, Z.; Xu, Y.; Li, L.; and Li, Z. 2020. View-dependent dynamic point cloud compression. *IEEE Transactions on Circuits and Systems for Video Technology*, 31(2): 765–781.